The Optical Light Curve of GRB 221009A: The Afterglow and the Emerging Supernova

M. D. Fulton[1] , S. J. Smartt[1,2] , L. Rhodes[2] , M. E. Huber[3] , V. A. Villar[4,5,6] , T. Moore[1] , S. Srivastav[1] ,
A. S. B. Schultz[3] , K. C. Chambers[3] , L. Izzo[7] , J. Hjorth[7] , T.-W. Chen[8,9] , M. Nicholl[10] , R. J. Foley[11] ,
A. Rest[12,13] , K. W. Smith[1] , D. R. Young[1] , S. A. Sim[1] , J. Bright[2] , Y. Zenati[13] , T. de Boer[3] , J. Bulger[3] , J. Fairlamb[3] ,
H. Gao[3] , C.-C. Lin[3] , T. Lowe[3] , E. A. Magnier[3] , I. A. Smith[14] , R. Wainscoat[3] , D. A. Coulter[11] , D. O. Jones[15] ,
C. D. Kilpatrick[16] , P. McGill[11] , E. Ramirez-Ruiz[11] , K.-S. Lee[17] , G. Narayan[18,19] , V. Ramakrishnan[17] ,
R. Ridden-Harper[20] , A. Singh[21] , Q. Wang[13] , A. K. H. Kong[22] , C.-C. Ngeow[23] , Y.-C. Pan[23] , S. Yang[24] ,
K. W. Davis[11] , A. L. Piro[25] , C. Rojas-Bravo[11] , J. Sommer[1,26] , and S. K. Yadavalli[4,5,6]

[1] Astrophysics Research Centre, School of Mathematics and Physics, Queen's University Belfast, BT7 1NN, UK; mfulton07@qub.ac.uk
[2] Department of Physics, University of Oxford, Denys Wilkinson Building, Keble Road, Oxford OX1 3RH, UK
[3] Institute for Astronomy, University of Hawai'i, 2680 Woodlawn Drive, Honolulu, HI 96822, USA
[4] Department of Astronomy and Astrophysics, Pennsylvania State University, 525 Davey Laboratory, University Park, PA 16802, USA
[5] Institute for Computational & Data Sciences, The Pennsylvania State University, University Park, PA 16802, USA
[6] Institute for Gravitation and the Cosmos, The Pennsylvania State University, University Park, PA 16802, USA
[7] DARK, Niels Bohr Institute, University of Copenhagen, Jagtvej 128, DK-2200 Copenhagen, Denmark
[8] Technische Universität München, TUM School of Natural Sciences, Physik-Department, James-Franck-Straße 1, D-85748 Garching, Germany
[9] Max-Planck-Institut für Astrophysik, Karl-Schwarzschild Straße 1, D-85748 Garching, Germany
[10] Birmingham Institute for Gravitational Wave Astronomy and School of Physics and Astronomy, University of Birmingham, Birmingham B15 2TT, UK
[11] Department of Astronomy and Astrophysics, University of California Santa Cruz, 1156 High St., Santa Cruz, CA 95060, USA
[12] Space Telescope Science Institute, 3700 San Martin Drive, Baltimore, MD 21218, USA
[13] Department of Physics and Astronomy, The Johns Hopkins University, Baltimore, MD 21218, USA
[14] Institute for Astronomy, University of Hawai'i, 34 Ohia Ku St., Pukalani, HI 96768-8288, USA
[15] Gemini Observatory, NSF's NOIRLab, 670 N. A'ohoku Place, Hilo, Hawai'i, 96720, USA
[16] Center for Interdisciplinary Exploration and Research in Astrophysics (CIERA), Northwestern University, 1800 Sherman Ave, Evanston, IL 60201, USA
[17] Department of Physics and Astronomy, Purdue University, 525 Northwestern Avenue, West Lafayette, Indiana 47907, USA
[18] Department of Astronomy, University of Illinois at Urbana-Champaign, 1002 W. Green St., IL 61801, USA
[19] Center for Astrophysical Surveys, National Center for Supercomputing Applications, Urbana, IL 61801, USA
[20] School of Physical and Chemical Sciences—Te Kura Matū, University of Canterbury, Private Bag 4800, Christchurch 8140, New Zealand
[21] Departamento de Ciencias Fisicas, Facultad de Ciencias Exactas, Universidad Andres Bello, Fernandez Concha 700, Las Condes, Santiago, Chile
[22] Institute of Astronomy, National Tsing Hua University, Hsinchu 30013, Taiwan
[23] Graduate Institute of Astronomy, National Central University, 300 Jhongda Road, 32001 Jhongli, Taiwan
[24] Department of Astronomy, The Oskar Klein Center, Stockholm University, AlbaNova, SE-10691 Stockholm, Sweden
[25] The Observatories of the Carnegie Institution for Science, 813 Santa Barbara St., Pasadena, CA 91101, USA
[26] Universitäts-Sternwarte München, Fakultät für Physik, Ludwig-Maximilians Universität München, Scheinerstr. 1, D-81679 Munich, Germany

Abstract

We present extensive optical photometry of the afterglow of GRB 221009A. Our data cover 0.9–59.9 days from the time of Swift and Fermi gamma-ray burst (GRB) detections. Photometry in *rizy*-band filters was collected primarily with Pan-STARRS and supplemented by multiple 1–4 m imaging facilities. We analyzed the Swift X-ray data of the afterglow and found a single decline rate power law $f(t) \propto t^{-1.556 \pm 0.002}$ best describes the light curve. In addition to the high foreground Milky Way dust extinction along this line of sight, the data favor additional extinction to consistently model the optical to X-ray flux with optically thin synchrotron emission. We fit the X-ray-derived power law to the optical light curve and find good agreement with the measured data up to 5−6 days. Thereafter we find a flux excess in the *riy* bands that peaks in the observer frame at ∼20 days. This excess shares similar light-curve profiles to the Type Ic broad-lined supernovae SN 2016jca and SN 2017iuk once corrected for the GRB redshift of $z = 0.151$ and arbitrarily scaled. This may be representative of an SN emerging from the declining afterglow. We measure rest-frame absolute peak AB magnitudes of $M_g = -19.8 \pm 0.6$ and $M_r = -19.4 \pm 0.3$ and $M_z = -20.1 \pm 0.3$. If this is an SN component, then Bayesian modeling of the excess flux would imply explosion parameters of $M_{ej} = 7.1^{+2.4}_{-1.7}\ M_\odot$, $M_{Ni} = 1.0^{+0.6}_{-0.4}\ M_\odot$, and $v_{ej} = 33,900^{+5900}_{-5700}$ km s^{-1}, for the ejecta mass, nickel mass, and ejecta velocity respectively, inferring an explosion energy of $E_{kin} \simeq 2.6$–9.0×10^{52} erg.

Unified Astronomy Thesaurus concepts: Gamma-ray bursts (629); Type Ic supernovae (1730); Light curves (918); X-ray photometry (1820); Optical astronomy (1776)

Supporting material: data behind figure

1. Introduction

Long-duration gamma-ray bursts (lGRBs) are typically associated with the signature of a broad-lined Type Ic supernova (SN) in their light curves and spectra, as the afterglow fades and an SN rises within 10–20 days. Since the

Table 1
Depths of the 3π Reference Images Used for PS2 Image Data Template Subtraction

Filter	Exposure Time (s)	3σ Depth		A_λ^{MW} (mag)	A_λ^{Tot} (mag)	λ_{obs} (nm)	λ_{rest} (nm)
		AB Mag	Flux (μJy)				
r_{PS}	636	>22.24	<4.61	3.497	4.64	617	536
i_{PS}	930–1020	>22.01	<5.70	2.590	3.44	752	653
z_{PS}	540–570–600	>21.14	<12.71	2.036	2.70	866	752
y_{PS}	620	>20.34	<26.54	1.674	2.22	962	836

Note. The effective wavelengths of the Pan-STARRS filters are from Tonry et al. (2012) and the corresponding rest-frame wavelengths at $z = 0.151$ are listed. The Galactic foreground extinction (A_λ^{MW}) in each filter is from Schlafly & Finkbeiner (2011) and the total extinction required for the observed X-ray to optical flux ratio is A_λ^{Tot}.

discovery of SN 1998bw/GRB 980425 and SN 2003dh/GRB 030329 (Galama et al. 1998; Hjorth et al. 2003) more than 40 probable GRB-SNe have been observed (e.g., Hjorth & Bloom 2012; Cano et al. 2017a). However, an SN signature is not always detected for nearby lGRBs (Della Valle et al. 2006; Fynbo et al. 2006), leading to speculation that massive stellar deaths are not the source of all lGRBs (Leśniewska et al. 2022; Rastinejad et al. 2022).

GRB 221009A was first detected and announced by the Neil Gehrels Swift Observatory via the Gamma-ray Coordinates Network (GCN) circulars (Dichiara et al. 2022). A hard X-ray source and an optical counterpart at Swift-UVOT white light magnitude 16.63 were reported, locating it within the Galactic plane at a latitude of $b = 4°.322$. The lGRB nature was confirmed by Kennea & Williams (2022), while the Gamma-ray Burst Monitor (GBM), on board the Fermi spacecraft, reported a detection 1 hr before the Swift trigger time (Veres et al. 2022), noting it was the brightest GRB ever detected by Fermi-GBM instrument. Fermi's Large Area Telescope (LAT) further reported the detection of the GRB and recorded its highest-energy photon at 7.8 GeV (Bissaldi et al. 2022). The first ground-based detections of the afterglow in the optical by Perley (2022) and in the radio by Bright et al. (2022) were followed by a multitude of GCN circulars reporting measurements across the electromagnetic spectrum. Interest in this extraordinary event further increased when the LHAASO experiment reported the detection of more than 5000 very-high-energy (VHE) photons with energies up to 18 TeV (Huang et al. 2022). The Carpet-2 experiment reported a possible 251 TeV photon detection (Dzhappuev et al. 2022), which would be remarkable if proven reliable. Spectra of the afterglow were obtained by de Ugarte Postigo et al. (2022) and Castro-Tirado et al. (2022), both of which reported a red continuum with absorption features that correspond to Ca II, Ca I, Na I D at a redshift of $z = 0.151$. A host was later confirmed, and a similar redshift of $z = 0.151$ was determined by Izzo et al. (2022) through the identification of host-galaxy absorption and emission lines. At this extragalactic distance, such VHE photons should be absorbed through pair production when they scatter off the extragalactic background light, raising the possibility of axion-like particle production (Baktash et al. 2022; Carenza & Marsh 2022). The remarkably high fluence, luminosity and detection of VHE photons make GRB 221009A an object of broad interest.

In this Letter, we propose the detection of an SN signature in the fading afterglow of GRB 221009A, the brightest GRB known to date. We present an extensive photometric data set primarily from the Pan-STARRS2 Observatory, supported by multiple other facilities. The search for an SN signal is

complicated due to the high, and uncertain, foreground extinction, the bright afterglow, and the uncertainty in host-galaxy contribution. Throughout this Letter, we assume a GRB detection time of $T_0 = 59861.55347$ (2022 October 9 at 13:16:59.99 UT) from Fermi (Veres et al. 2022), a Hubble Constant of $H_0 = 70\,\mathrm{km\,s^{-1}\,Mpc^{-1}}$ and the redshift of $z = 0.151$ (Castro-Tirado et al. 2022; de Ugarte Postigo et al. 2022; Izzo et al. 2022). This corresponds to a luminosity distance of $D_L = 718\,\mathrm{Mpc}$ and distance modulus $\mu = 39.28$ assuming a flat universe with $\Omega_M = 0.3$.

2. Observational Data

The Pan-STARRS (PS) system comprises two 1.8 m telescope units located at the summit of Haleakala on the Hawaiian island of Maui (Chambers et al. 2016). The Pan-STARRS1 (PS1) telescope is fitted with a 1.4 Gigapixel camera (GPC1) with 0″.26 arcsec pixels providing a 3°.0 diameter focal plane, corresponding to a field-of-view area of 7.06 deg². The Pan-STARRS2 (PS2) telescope is fitted with a similar but larger 1.5 Gigapixel camera (GPC2) resulting in a slightly wider field of view. Both telescopes are equipped with a Sloan Digital Sky Survey (SDSS)–like filter system, denoted as $grizy_{P1}$. The Pan-STARRS1 Science Consortium (PS1SC) 3π Survey produced $grizy_{P1}$ images of the whole sky north of $\delta = -30°$ (Chambers et al. 2016). Multiepoch observations spanning 2009–2014 have been stacked and a public data release provides access to the images and catalogs (Flewelling et al. 2020). These data provide reference images for immediate sky subtraction, which allows the discovery of transients and accurate photometry with host-galaxy removal. Pan-STARRS data from both telescopes are processed in real time as described in Magnier et al. (2020a, 2020b) and Waters et al. (2020) at the University of Hawaii and the transient sources are selected, filtered, and classified by the Transient Science Server at Queen's University Belfast (Smith et al. 2020). In normal survey and discovery mode, these feed science programs such as the Young Supernova Experiment (Jones et al. 2021) and the Pan-STARRS Search for kilonovae (McBrien et al. 2021).

The Pan-STARRS afterglow observations of GRB22100A presented here were all taken with PS2. After the discovery of the GRB and the optical afterglow, we triggered PS2 to observe in r_{PS}, i_{PS}, z_{PS}, and y_{PS}, with a nightly sequence between 2022 October 11 and December 4 (Huber et al. 2022), depending on Moon phase and weather. Photometry was carried out on the difference images with the Pan-STARRS1 3π sky survey data (Chambers et al. 2016) used as references. The 3π data are made of stacks of short exposures and the total exposure times and depths at the position of the afterglow (which we measure

at R.A. = 288°26459 decl. = +19°77341) are listed in Table 1. The photometric zero points on the PS2 target images were set with the Pan-STARRS1 3π catalog (Flewelling et al. 2020). We typically used 100–200 s exposures and stacked images on any one night (from 1 to 12 images, depending on target magnitude and sky brightness).

Two methods were used to measure the flux on the difference images. A difference image was created from each individual exposure, and a point-spread function (PSF) was forced at the GRB 221009A afterglow position (measured from the early, bright epochs). We statistically combined the measured PSF flux from each difference image through a weighted average, using a temporal bin size of 1 day. For the later Pan-STARRS epochs ($t - T_0 > 34$ days) we increased the bin size to 4 days in the zy filters to enhance the signal-to-noise. Alternatively, an image stack on each night was created, and a difference image produced from the stack. Again, a PSF was forced at the GRB afterglow position and flux measurement used. All fluxes and magnitudes quoted here are in microjanskys (μJy) and AB magnitudes. The results from image stacking were used instead of the weighted average of fluxes only when the object fell on a masked chip within the camera CCD, which prevented the typical pipeline processing of target images described in Chambers et al. (2016). Regardless of the method, the resulting flux measurements were calibrated carefully to the Pan-STARRS1 DR2 3π reference catalog (Flewelling et al. 2020) using approximately 1000 field stars visible within the target frames.

While most of the data here are provided by PS2, we gathered other important photometric data with the 0.4 m Ritchey–Chrétien Super Light Telescope (SLT; Chen et al. 2022) and Cassegrain Lulin One-meter Telescope (LOT) at the Lulin Observatory, Taiwan; the Dark Energy Camera (DECam) on the 4 m Telescope at the Cerro Tololo Inter-American Observatory, Chile; the 4.1 m Southern Astrophysical Research (SOAR) Telescope, Chile; the 1 m Swope Telescope, Chile; the IO:O on the 2.2 m Liverpool Telescope (LT), La Palma; and MegaCam on the 3.6 m Canada–France–Hawaii Telescope, Hawaii.

Eight epochs of DECam observations were conducted between 2022 October 16 (MJD 59,868.01) and 2022 October 31 (MJD 59,883.011) taking between 2 and 5×100 s exposures in the filters r and i. The data were reduced and photometrically calibrated with the photpipe package (Rest et al. 2014) using the images from 2022 October 16 as templates. These were subtracted from all subsequent images and a PSF was forced at the afterglow position on the difference images. Since the template contains transient flux and we were not able to get a final set of templates in which the afterglow had faded, we applied an offset to match the DECam r-filter flux measured on MJD 59,880.01 to the SOAR epoch on MJD 59,880.02, and the DECam i-filter flux measured on MJD 59,875.01 to the PS2 epoch on MJD 59,875.23. These offsets were subsequently applied to all the DECam difference images in the respective filters. Data from Swope were subjected to difference imaging, using the Pan-STARRS1 3π references as templates and forced photometry was implemented thereafter.

We used the three epochs of Hubble Space Telescope (HST) data that are publicly available through the DDT program of Levan et al. (2022). The WFC3 passbands of the F625W, F775W, and F098M filters are similar to that of the r_{PS}, i_{PS}, and

y_{PS} filters respectively (see Section 4). PSF magnitudes were measured on the HST target images using the DOLPHOT package (Dolphin 2016). Observations conducted by SLT, LOT, SOAR, LT, and MegaCam between October 10 and November 8 were not subjected to any form of image subtraction; instead, a PSF was forced onto the target images using python packages, *Astropy* and *Photutils*,[27] and the resulting flux measurements were calibrated against Pan-STARRS1 3π survey field stars.

Since no difference imaging was applied to the SLT, LOT, SOAR, or LT one may be concerned by late-time host-galaxy flux contamination. This is particularly concerning when the measured flux of the transient is comparable to, or fainter than, the limits we can put on the host galaxy from the Pan-STARRS1 3π data (see Table 1). However, the photometry between different instruments (with and without difference imaging) is consistent within the statistical uncertainties. A probable faint host galaxy is visible in the deepest F625W and F775W HST images, approximately 0″5 offset to the northeast. However, this is too faint to contribute significantly to the r and i photometry and our y_{PS} data are all image subtracted. Hence we make the assumption that there is no host-galaxy flux contributing to the nondifferenced images in the filters r, i, or z. This can only be confirmed with deep observations in the next observing season. We list our measurements also in fluxes (microjanskys) within Appendix A so that a future correction can be applied should that be necessary.

3. Analysis of the X-Ray and Optical Afterglow

The X-ray counterpart to GRB 221009A was observed by the Neil Gehrels Swift Observatory X-ray telescope (XRT) starting 0.9 hr after the Fermi trigger (Veres et al. 2022), and is still observing at the time of writing. We downloaded the Swift XRT data to date from the Swift Burst Analyser (Evans et al. 2007, 2009, 2010). A single decaying power law can best describe the XRT light curve. We fit a power-law component to the first 60 days of flux data, using the fluxes and not flux densities so as not to introduce any spectral bias, and found the light curve is described with $f(t) \propto t^{-1.556 \pm 0.002}$. There is no evidence of any breaks in the light curve that could result from either a spectral break (e.g., the cooling break) passing through the band or a jet break. There is also no evidence of a change in the X-ray photon index (related to the spectral index), indicating no significant spectral evolution occurring over the first 60 days postburst. The Swift Burst Analyser quotes an X-ray photon index of 1.78 ± 0.01, which corresponds to a spectral index ($S(\nu) \propto \nu^{\alpha}$) of $\alpha = -0.78 \pm 0.01$. The measured X-ray light-curve decay and spectral index indicate the X-ray emission originates from optically thin synchrotron radiation, where the synchrotron cooling break has a frequency that is higher than that of the observing band.

Given that the optical light curve is also showing a decay, and that only optically thin synchrotron radiation produces a decaying light curve within the fireball model, the optical emission should be on the same branch of the afterglow spectrum as the X-ray band and thus the decay rates should be identical (Sari et al. 1998; Granot & Sari 2002). A power-law decay also best describes the measured optical decay. However, the difference between the optical and X-ray decay rates is not

---

[27] Python tool used to measure PSF photometry can be found on GitHub. https://github.com/mnicholl/photometry-sans-frustration.
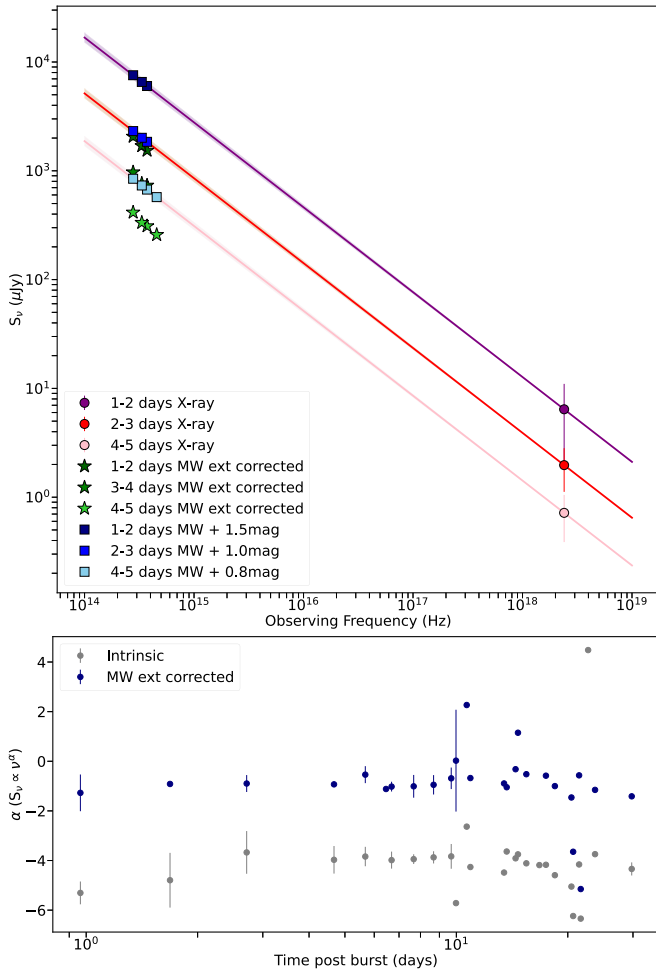
Figure 1. Upper panel: comparison of the X-ray flux densities (and photon index) with the optical flux densities corrected for the known Milky Way extinction (stars) for three epochs: +1–2, +2–3, and +4–5 days postburst. Also shown (squares) are the optical flux densities with an additional extinction correction such that it agrees with the X-ray spectrum. We estimate that at least another 0.8 mag of extinction (averaged across the optical bands) is required along the line of sight in addition to what is provided by the Milky Way extinction maps (Schlafly & Finkbeiner 2011). Lower panel: spectral-index fit to the optical bands at all wavelengths, both the observed and the Galactic extinction corrected points. Even after correcting for Galactic extinction, the optical spectral index is still too shallow to agree with the X-ray spectrum. This further suggests a need for an additional absorption component.

large enough to be consistent with the presence of a spectral break between the two bands. The difference in light-curve decay rates should be $1/4$ if the cooling break is between the optical and X-ray bands and accompanied by a spectral-index difference of $1/2$ (Granot & Sari 2002).

In addition to differing light-curve decay rates, the optical flux densities do not agree with what is predicted from the X-ray spectrum (Figure 1). This is the result of the line-of-sight extinction through the Galactic plane being high at $A_V = 4.223$ (Schlafly & Finkbeiner 2011). We confirm that the extinction is high by measuring an optical spectral index of ($\alpha \approx -4$), which is notably steeper than the expected and measured X-ray spectral index of the synchrotron emission, $\alpha \approx -0.8$. We correct the optical data for the Galactic extinction across the specific $rizy_{PS}$ filters as reported in the NASA Extragalactic Database (NASA/IPAC Extragalactic Database (NED) 2019), which uses the maps of Schlafly & Finkbeiner (2011) and the Fitzpatrick (1999) reddening law (see Table 1). Figure 1 shows

the X-ray to optical spectral energy distribution (SED). Once corrected for Galactic extinction (only), the optical flux densities are still too faint to agree with the extrapolation of the X-ray data using a spectral index of $S(\nu) \propto \nu^{-0.78\pm0.01}$. Additional extinction is required and the amount required to reconcile the optical ad X-ray fluxes varies across the three epochs shown in Figure 1. The optical spectral index (Figure 1) is also lower than the expected $\alpha \simeq -0.8$, further supporting a requirement for a source of extra extinction.

The earliest epoch (1–2 days postburst) requires 1.5 mag of extra extinction, reducing to 1.0 (at 2–3 days) and 0.8 mag (4–5 days). It is not clear why the implied extra extinction would vary across the three epochs but time-variable extinction has been proposed before (e.g., GRB 190114C; Campana et al. 2021; Melandri et al. 2022). We use the value of 0.8 mag (which is the average value across the $rizy_{PS}$ bands) as this is the closest value in time to the possible emergent SN signal. There are three possibilities. for this additional line-of-sight extinction. The Galactic dust structure may not be accurately captured by the low resolution Milky Way extinction maps of Schlafly & Finkbeiner (2011) or it is possible that $R_V > 3.1$, which may be plausible in this high-density region. The third possibility is additional absorption in the host. This may not be surprising given four of the five GRBs with VHE detections ($E_\gamma > 100$ GeV) also have evidence of strong dust contamination as mentioned in Rhodes et al. (2022). The VHE GRBs appear to have an increased likelihood of dust absorption compared to the rest of the long GRB population where only about 25% of events have significant optical extinction (Chandra & Frail 2012).

We plot our optical data in AB magnitudes in Figure 2, including all points with $\geqslant 2\sigma$ significance. We first measured the optical decay rate in all filters independently and across all epochs ($T_0 + 1 < t \lesssim T_0 + 56$). The decay rate in the ri filters follow $f(t) \propto t^{-1.43\pm0.02}$, the z filter follows $f(t) \propto t^{-1.54\pm0.02}$, and the y filter follows $f(t) \propto t^{-1.21\pm0.01}$. There is not a single decaying term that can describe the fade in all filters, and, with the exception of the z filter, the decay terms derived are substantially shallower than that of the X-ray slope. Using epochs from ($1 \leqslant t - T_0 \leqslant 4.7$ d) in the izy_{PS} filters, we also fit the X-ray derived slope of $f(t) \propto t^{-1.556\pm0.002}$ to these points. In the r_{PS} filter, we lack data at 2–3 days so we extend the temporal baseline to include the 6.7 d PS2 point. We find the early data are well explained by the model, as evidenced by the measured normalized chi-squared value of $\chi_n^2/\mathrm{dof} = 0.4/6.0$.

The dissimilar decaying rates between the optical filters, and the deviation of the optical light curve from the X-ray light curve starting at $t - T_0 > 7$ days are suggestive of another component appearing in the data. The light-curve deviation is most pronounced in the y_{PS} filter at $t - T_0 = 21$ days, and we discuss this in the next section. Figure 3 illustrates the data quality and detections around the peak of the flux excess in the PS2 images, for which we have deep reference images from the 3π survey (Chambers et al. 2016).

4. Interpretation of the Excess Flux as a Supernova Signature

To determine if the excess flux observed starting from ~ 7 to 8 days is consistent with a Type Ic broad-lined SN (Ic-BL) contribution, we compare the excess to the riz light curve of SN 2016jca from Cano et al. (2017b) and the $griz$ light curve of SN 2017iuk from Izzo et al. (2019). SN 2016jca was a Type Ic-BL that emerged in GRB 161219B (Cano et al. 2017b), at a
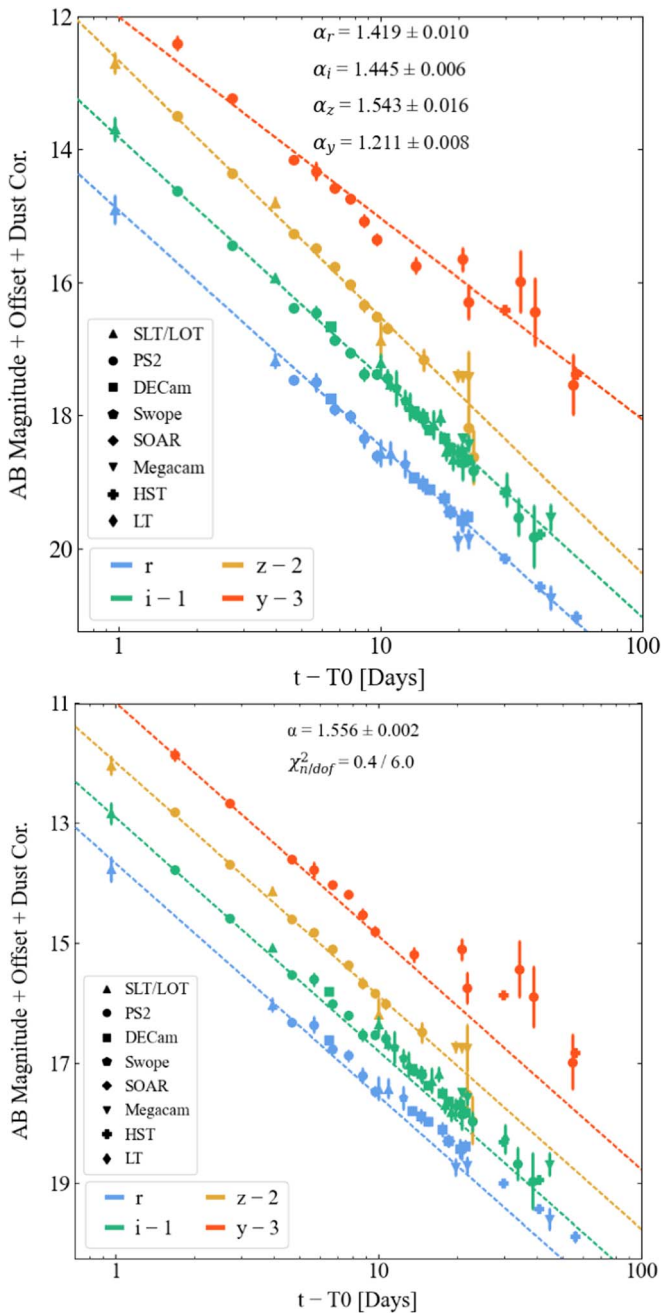
Figure 2. Upper panel: the optical afterglow of GRB 221009A in the *rizy* filters. A decaying power law has been fit to each filter independently using the measurements across all epochs, which have been corrected for galactic dust extinction, and only magnitude measurements with $\geqslant 2\sigma$ significance are shown. The data points are in the observer frame with the instruments and telescopes as in the legend. Bottom panel: the same optical afterglow of GRB 221009A, this time with a single power law of $f(t) \propto t^{-1.556}$ (derived from the X-ray measurements) fit to all filters using only data points up to 7 days after GRB trigger, which have been corrected for galactic dust extinction plus extra extinction required by X-ray analysis.

(The data used to create this figure are available.)

redshift of $z = 0.1475$. This redshift is almost identical to GRB 221009A, and as such, the *riz* light curve can be compared directly. SN 2017iuk was another Type Ic-BL that emerged in GRB 171205A. It is the only Type Ic-BL with published rest-frame z-band filter coverage, to compare to the observer frame y_{PS} data of GRB 221009A. At this redshift, the

GROND griz SDSS filters (Fukugita et al. 1996) correspond to the observer frame of the Pan-STARRS system $rizy_{PS}$ filters at $z = 0.151$ to a good approximation (see Table 1). In particular, the rest-frame z-band transforms to the observed y_{PS} filter and since the y_{PS} data apparently show the strongest excess, the z-band rest-frame data are essential.

We used the observed data of GRB 171205A and SN 2017iuk listed in Izzo et al. (2019) which is already corrected for host-galaxy contribution, and we further corrected for dust extinction to the SN. We do not subtract off any Xray-derived power law as the afterglow contribution represented by this is considerably less than the SN contribution, as early as 3 days after explosion. As the light curve of 2017iuk is only $\sim$27 days long, we generated a continuous model light-curve fit up to 100 days after explosion using a Markov Chain Monte Carlo Bazin fit (Bazin et al. 2009) for each of the griz data.

To obtain the light curve of SN 2016jca, we used the observed data listed in (Cano et al. 2017b) and subtracted off an X-ray-derived power law of $f(t) \propto t^{-0.79}$ fitted to the early-time data $(t - T_0 < 1$ day$)$ to remove the GRB 161219B afterglow contribution. We also corrected for the host-galaxy contribution (using the same host flux determined by Cano et al. 2017b) and dust extinction to the SN. The light curve of SN 2016jca is well sampled up to 70 days after explosion, and so we did not require a Bazin fit here.

These light curves were then adjusted accordingly for extinction along the line of sight to GRB 221009A and time dilation to the GRB redshift of $z = 0.151$. We used the total estimated line-of-sight extinction implied from the X-ray to optical power-law slope as derived in Section 3 (which is higher than that from Milky Way only), explicitly $A_r = 4.64$, $A_i = 3.44$, $A_z = 2.70$, $A_y = 2.22$. These light-curve fluxes of SN 2016jca and SN 2017iuk were subsequently added to the X-ray power-law slope derived in Section 3 and overlaid onto the GRB afterglow in Figure 4.

The light-curve fluxes of SN 2016jca required moderate (arbitrary) scaling to produce a power law plus SN component that quite satisfactorily matches the observed data of GRB 221009A. Scaling factors of 2.0 and 1.6 were used for the r filter and i filter respectively. We computed Bayes factors to compare the continuation of the imposed X-ray power law to the power law plus an SN component. We found factors of 3.4 and 7.5 for the r filter and i filter respectively. This favors a model with a power law plus SN rather than the imposed X-ray power law only. The light-curve shape and peak magnitudes are similar (within the errors) to that of SN 2016jca (Cano et al. 2017b; Ashall et al. 2019). We estimate rest-frame, absolute magnitudes of $M_g = -19.7 \pm 0.6$ and $M_r = -19.6 \pm 0.3$ for a Ic-BL SN component of similar nature to SN 2016jca.

The SN 2017iuk light-curve model fluxes in the griz filters required considerable scaling (arbitrarily) to match the corresponding observed fluxes of GRB 221009A in the $rizy_{PS}$ bands. We require scaling factors in the rest-frame grz filters of 4.8, 1.9, and 4.6, respectively, to match the excess flux observed in the GRB data. This would produce peak magnitudes of $M_g = -19.9 \pm 0.6$ and $M_r = -19.3 \pm 0.3$ and $M_z = -20.1 \pm 0.3$ for the SN component inside GRB 221009A. No consistent single scaling factor can produce the colors and peak magnitudes in all filters. However, the variation in color of Type Ic SNe and the uncertain extinction toward GRB 221009A (both Milky Way and the additional required extinction) may explain why differences are found in each filter. We note that a difference in scaling factors was considered in the Cano et al. (2017b) interpretation of
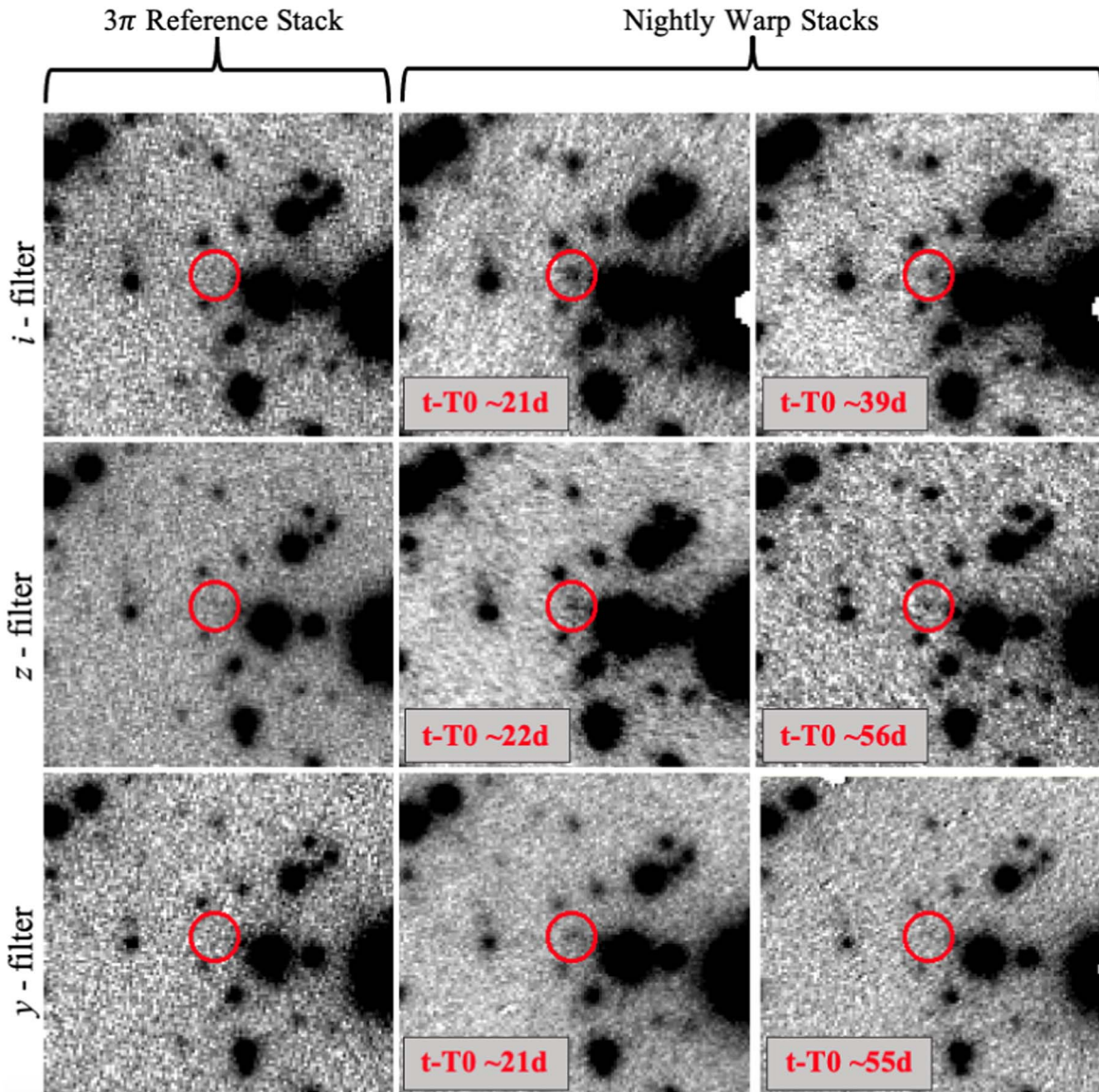
Figure 3. Pan-STARRS reference images and detections. Top triplet: $i_{\rm PS}$ filter reference image, intranight stacks from MJD 59,882 (+21 days, around SN peak) and MJD 59,900 (+39 days). Middle triplet: $z_{\rm PS}$ filter reference image, intranight stacks from MJD 59,883 (+22 days) and MJD 59,917 (+56 days). Bottom triplet: $y_{\rm PS}$ filter reference image, intranight stacks from MJD 59,882 at (+21 days, around SN peak), and MJD 59,916 (+55 days). Location of GRB 221009A is centered inside the red circle.

SN 2016jca. We computed Bayes factors (in the same way as for the SN 2016jca comparison) and found 3.4, 7.4, and 3.9 for the grz filters respectively. We emphasize that this is comparing the imposed X-ray power law (no SN) to the power law plus SN component after 7 days. Again, this method favors a Ic-BL component, but only with these assumptions.

We do not measure a peak absolute magnitude in the observer frame z filter for either SN comparison, as the Bayes factors from such comparisons strongly favored a "no SN" solution regardless of the scaling factors used. We also considered a scenario without the extra dust extinction suggested by the X-ray analysis. In this, we measure peak absolute magnitudes of $M_g = -18.7 \pm 0.6$, $M_r = -18.6 \pm 0.3$, and $M_z = -19.6 \pm 0.3$ from the SN 2017iuk comparison and $M_g = -18.6 \pm 0.6$, $M_r = -18.7 \pm 0.3$ from the SN 2016jca comparison.

We subtracted the afterglow (X-ray power law) from the observed data and measured the color of the flux excess at two phases: peak brightness ($t - T_0 \sim 21$ days) and at late times

($t - T_0 \sim 34$ days), to check for a color change which may be indicative of an SN component. Using only measurements made through difference imaging to mitigate host contribution, and discounting dust extinction, we measure observed $i - y$ colors ($r - z$ in the rest frame) of $i - y = 2.77 \pm 0.56$ and $i - y = 4.24 \pm 1.95$ at peak brightness and late times, respectively. The relatively large errors imply no meaningful color evolution can be interpreted.

To investigate why no apparent excess flux is visible in the observer frame z filter (rest-frame i filter), we took the spectrum of SN 1998bw and SN 2017iuk at peak and reddened both with the total extinction that we estimated in Section 2 ($A_V = 5.3$) and redshifted it to $z = 0.151$. These are plotted in Figure 5 along with the convolution of the spectra with the effective transmission curves of the filters used.[28] At $z = 0.151$, the

---

[28] Transmission profiles for all filters were obtained from the Spanish Virtual Observatory Filter Profile Service: http://svo2.cab.inta-csic.es/theory/fps.
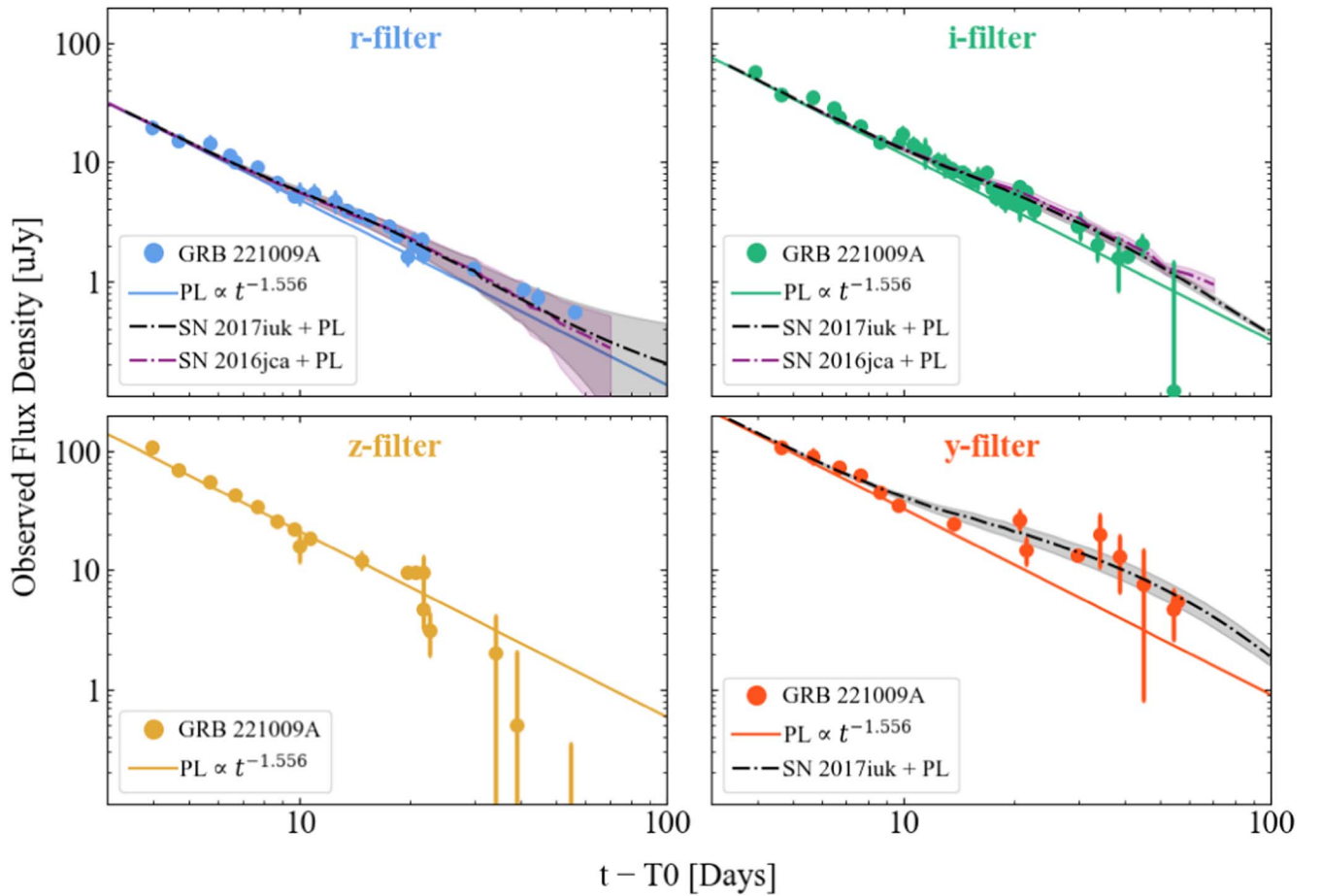
Figure 4. A multipanel plot of the light curve of GRB 221009A in microjanskys with the X-ray defined power-law fit (PL) of $f(t) \propto t^{-1.556 \pm 0.002}$. All forced photometry measurements are included, irrespective of significance. The redshifted and reddened light curves of SN 2016jca and SN 2017iuk have been combined with flux from the X-ray power-law model and further stretched in flux to depict the SN signature within GRB 221009A. Shaded regions depict the combined error associated with the SN measurements, power-law modeling, and dust extinction.

strong Ca II triplet has the deep P-Cygni absorption precisely at the position of the z_{PS} filter. The i_{PS} filter and the y_{PS} filter cover the emission peaks of the Ca II triplet and the 7500 Å blend. This may explain why there is little to no sign of a Ic-BL supernova signature in the z filter but is plausibly detected in the other filters.

We conclude that the excess flux above the extrapolation of the afterglow power law of $f(t) \propto t^{-1.556 \pm 0.002}$ can be explained by the emergence of an SN similar in luminosity and duration to the observed Type Ic-BL SNe SN 2016jca and SN 2017iuk. This SN associated with GRB 221009A would be labeled SN 2022xiw as reported on the IAU Transient Name server (Postigo et al. 2022). At the later epochs, our PS2 images have a depth and sensitivity close to those of the reference images we use for image subtraction. We demonstrate the reality of the detections compared with the PS1 3π stacks at several important epochs in Figure 3.

We compare our r- and i-filter photometry with original data (not GCN values) in Laskar et al. (2023), Shrestha et al. (2023) and Levan et al. (2023), three papers that suggest there is no strong evidence for an SN component in the data. Their data are in excellent agreement with ours, even though no image subtraction was undertaken. The z-filter data of Laskar et al. (2023) and Shrestha et al. (2023) are slightly brighter than ours after 8–10 days, which may suggest some host-galaxy contribution affects their measurements. The converted y filter

from the HST data of Levan et al. (2023) are fainter than ours by ~0.3 mag at the respective epochs, which we attribute to the combined galaxy plus PSF fits of Levan et al. (2023). Neither group have extensive y-filter or photometric near-infrared data at >10 days. While Kann et al. (2023) also claim no evidence for (or against) an SN component, their measurements include only two epochs of their own data beyond 10 days and no meaningful comparison is possible with our data set.

It appears that an SN component is only detectable with extensive and accurate photometric coverage beyond 10 days and assuming the X-ray power law is applied to the optical data (which may be disputed, e.g., Laskar et al. 2023). If we were to assume there is no SN component and that there is a break in the afterglow SED between the X-ray and optical decline rates, then, by applying similar extinction corrections, we find almost identical agreement with Laskar et al. (2023), Shrestha et al. (2023), and Levan et al. (2023) in the power-law decline rates for the riz filters across all epochs (see top panel of Figure 2), even though our data is better sampled and extends further in time. However, it is not possible to fit our y filter with the same single decaying power law derived from the riz filters, which would imply the achromatic behavior in the afterglow. Although, we acknowledge that if we were to replace our HST y-filter measurements with that reported in Levan et al. (2023), then we find it near possible to describe the y-filter
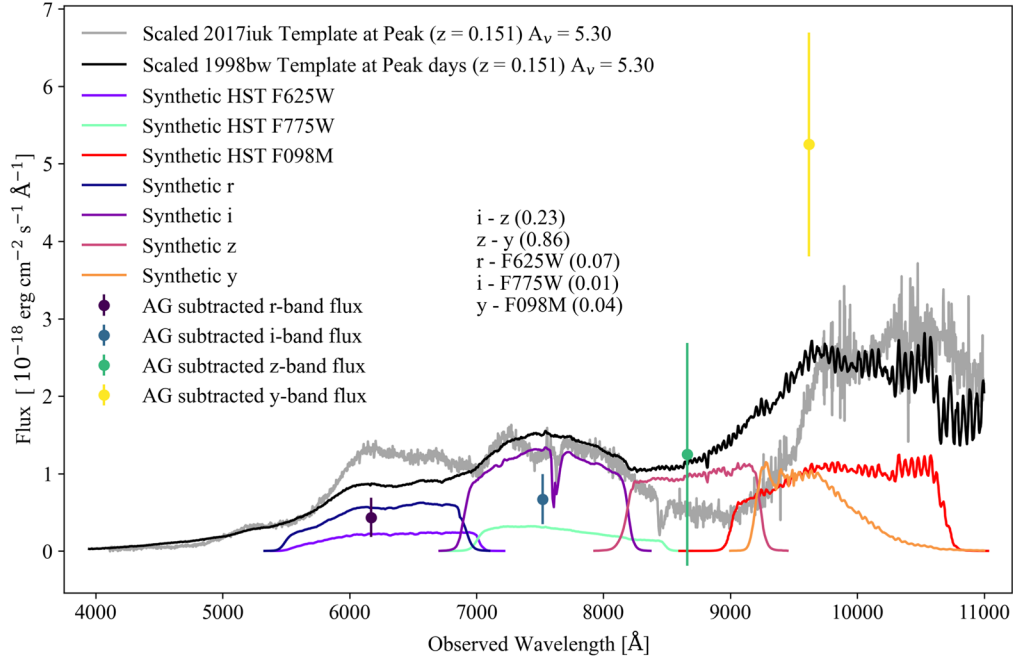
Figure 5. The spectrum of SN1998bw at peak (Patat et al. 2001) reddened with $A_V = 5.30$, redshifted to z = 0.151 and scaled to approximate the afterglow subtracted *rizy* flux at +20 days (after GRB), respectively. The convolution of the SN1998bw template with the transmission profiles of the filters used is overlaid. For comparison, following the same method, a scaled, reddened, and redshifted spectrum of SN 2017iuk at maximum light (Izzo et al. 2019) is also included.

decay with the same power law derived from the *riz* filters. We measure this single decaying power law as $f(t) \propto t^{-1.46\pm0.05}$.

5. Discussion and Conclusions

Given that the observational data of GRB 221009A and the emergence of an SN (SN 2022xiw) could be explained by the addition of scaled observed fluxes of two Type Ic-BL SNe, we can determine the physical parameters of SN 2022xiw. We model the afterglow subtracted SN signal to constrain the ejecta mass (M_{ej}), nickel mass (M_{Ni}) and ejecta expansion velocity (v_{ej}) using MOSFiT, an open-source, one-zone, semianalytical fitting tool for broadband SN light curves (Guillochon et al. 2018). MOSFiT employs dynesty, a nester sampling technique (Speagle 2020), to estimate posteriors of the fitted model. We use the default Arnett model within MOSFiT, which assumes that the SN is entirely powered by the radioactive decay of ^{56}Ni and ^{56}Co and assumes that the SED can be described by a blackbody (Arnett 1982; Villar et al. 2017). Assuming a constant gray opacity $\kappa = 0.07$ cm^{2}g^{-1} (Chugai 2000; Cano et al. 2017b) and flat priors on all fitted parameters, we find the posterior distributions returned are $M_{ej} = 5.6^{+1.1}_{-0.9}M_\odot$, $M_{Ni} = 0.5^{+0.20}_{-0.1}M_\odot$ and $v_{ej} = 35,500^{+4300}_{-4600}$ km s^{-1} to model the *riz*-band data of SN 2016jca (see Appendix B Figure 6). Errors quoted represent a 1σ width of the posterior distributions. The inferred explosion energy is then $E_{kin} \simeq 2.7$–6.3×10^{52} erg. These are broadly similar to those derived in the previous analysis of Cano et al. (2017b) and Ashall et al. (2019). Our M_{Ni} is higher, which we attribute to the different methods of fitting a bolometric light curve rather than the blackbody fitting of the selected filters.

Using the same set of priors, we model the *riy*-filter light curve of SN 2022xiw. The posterior distributions return the values $M_{ej} = 7.1^{+2.4}_{-1.7}\ M_\odot$, $M_{Ni} = 1.0^{+0.6}_{-0.4}\ M_\odot$, and $v_{ej} = 33,900^{+5900}_{-5700}$ km s^{-1}, (see Figure 7 in Appendix B), inferring explosion energy of $E_{kin} \simeq 2.6$–$.0 \times 10^{52}$ erg. These

are comparable to the quantities derived for SN 2016jca above but suggest a more energetic explosion and a larger mass of ^{56}Ni is required. This is reflected in the fact that the light-curve data of SN 2016jca requires modest scaling to reproduce the flux of SN 2022xiw. We test the robustness of our modeling by excluding the y_{PS}-band photometry (which may significantly deviate from our blackbody assumptions) and by excluding late-time observations (which may deviate from our assumption that the SN is in the photospheric phase). We find no statistically significant differences in derived properties from these tests.

The parameters of SN 2022xiw are similar to the more energetic Ic-BL SNe associated with lGRBs, termed hypernovae (Iwamoto et al. 1998; Mazzali et al. 2003). The sample of GRB-SNe has been reviewed and summarized by Hjorth & Bloom (2012) and more recently Wheeler et al. (2015) and Cano et al. (2017a). The latter studies suggest that GRB-SNe are characterized by the following average values: kinetic energies of $\overline{E_K} = 2.5 \times 10^{52}$ erg ($\sigma_{E_K} = 1.8 \times 10^{52}$), ejecta masses of $\overline{M_{ej}} = 6M_\odot$ ($\sigma_{M_\odot} = 4\ M_\odot$), and peak photospheric velocities of $\overline{v_{ph}} = 20,000M_\odot$ ($\sigma_{v_{ph}} = 8000\ M_\odot$). The most luminous GRB-SNe require ^{56}Ni masses of $0.5 \lesssim M_{Ni} \lesssim 0.9$, if the luminosity is powered by radioactivity.

The ^{56}Ni mass we derive ($M_{Ni} = 1.0^{+0.6}_{-0.4}\ M_\odot$), is on the high side of the known distribution of GRB-SNe. Similar to the SN 2016jca case above, we attribute this partly to fitting a computed bolometric light curve, which is made worse by the bright afterglow of GRB 221009A and the high, uncertain extinction creating considerable noise in the SN extracted flux. Nevertheless, the large uncertainty comfortably brackets GRB-SNe parameters previously derived.

Despite these uncertainties, the excess flux above the extrapolated afterglow leads us to conclude that there may be an SN signature in our ~60 day, well-sampled light-curve data of GRB 221009A (denoted SN 2022xiw), which is comparable
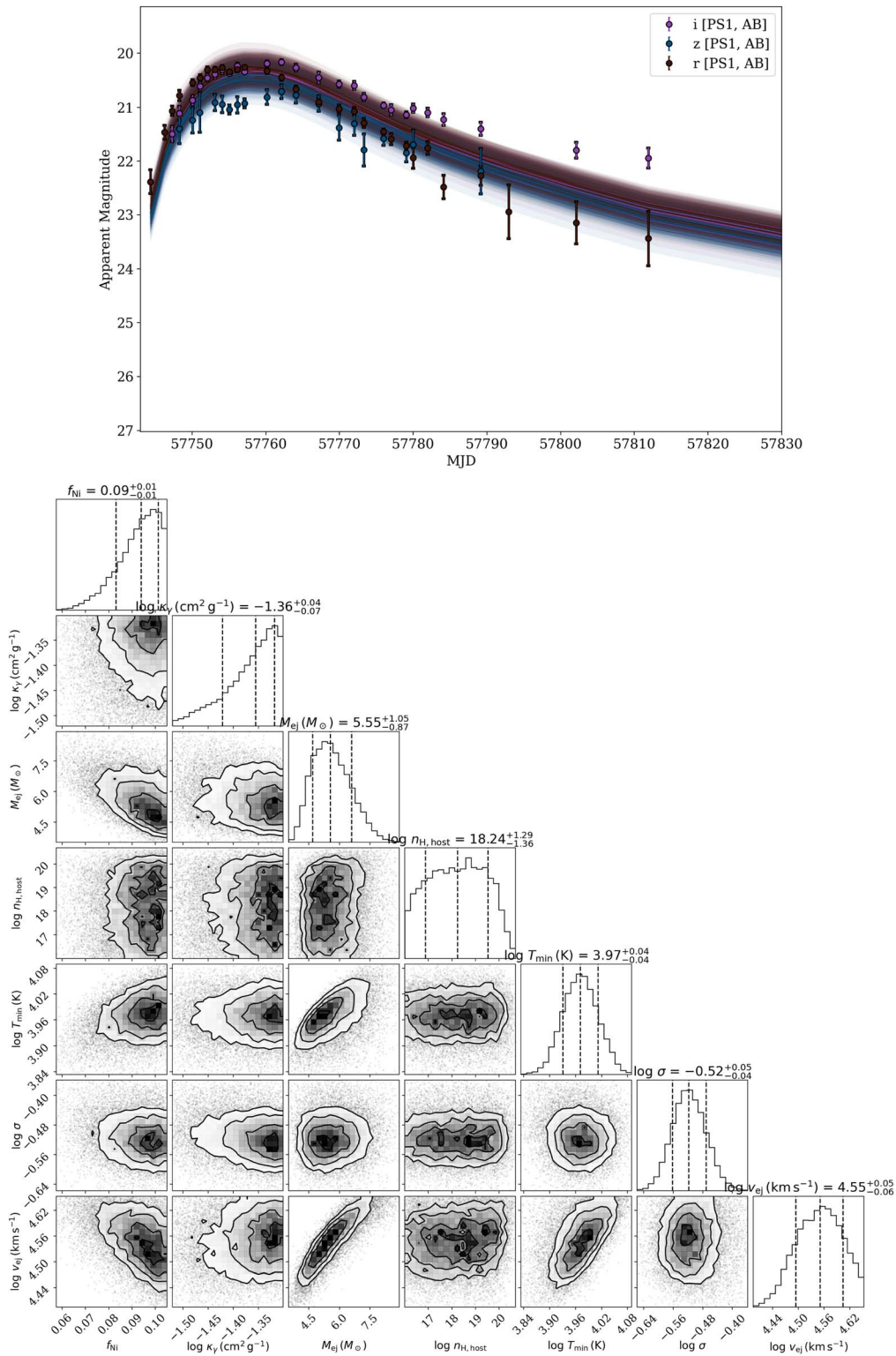
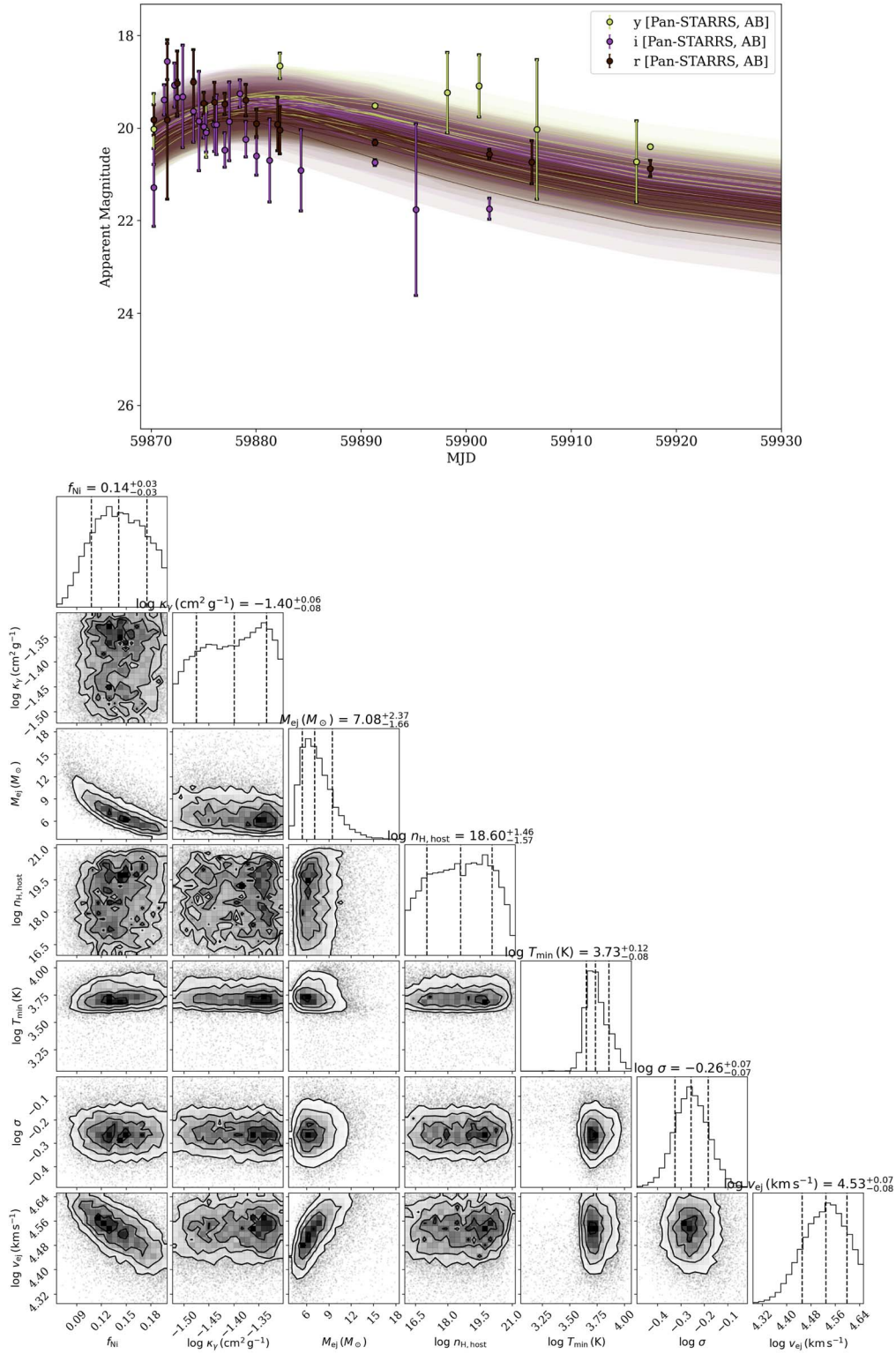**Figure 6.** Upper panel: MOSFiT light-curve models for SN 2016jca. Lower panel: derived parameters from the MOSFiT modeling.

in both luminosity and ejecta properties to other bright Type Ic-BL SNe events. To confirm, this will require a reanalysis of all multiwavelength data, to model the expected optical afterglow behavior.

Figure 7. Upper panel: MOSFiT light-curve models for SN 2022xiw. Lower panel: derived parameters from the MOSFiT modeling.

Appendix A
Photometry Data Table

A machine-readable file is provided, with all the photometry data for GRB 221009A behind Figures 2 and 4. Measurements are in AB magnitudes and microjanskys. All photometry is of the AG+SN and are uncorrected for galactic and host-galaxy dust extinction. Magnitude limits are quoted to 2σ. The total exposure time for each night is provided which is typically the sum of subexposures combined. The final column notes the method used to measure the fluxes for that particular epoch, i.e., stacked fluxes from individual difference images (*w-avr-flx*), stacked fluxes from individual difference images binned across multiple nights (*bw-avr-flx*), fluxes from a single stacked

difference image (*d-stack-flx*), or fluxes from a single stacked target image without differencing (*target-flx*).

Appendix B
Posterior Distributions for the Physical Parameters of SN 2016jca and SN 2022xiw

Here we show our light-curve models and posterior distributions for SN 2016jca and the proposed SN 2022xiw obtained through running MOSFiT (Guillochon et al. 2018). Specifics of the MOSFiT modeling are discussed in Section 5.

ORCID iDs

M. D. Fulton ⓘ https://orcid.org/0000-0003-1916-0664
S. J. Smartt ⓘ https://orcid.org/0000-0002-8229-1731
L. Rhodes ⓘ https://orcid.org/0000-0003-2705-4941
M. E. Huber ⓘ https://orcid.org/0000-0003-1059-9603
V. A. Villar ⓘ https://orcid.org/0000-0002-5814-4061
T. Moore ⓘ https://orcid.org/0000-0001-8385-3727
S. Srivastav ⓘ https://orcid.org/0000-0003-4524-6883
A. S. B. Schultz ⓘ https://orcid.org/0000-0003-4717-9119
K. C. Chambers ⓘ https://orcid.org/0000-0001-6965-7789
L. Izzo ⓘ https://orcid.org/0000-0001-9695-8472
J. Hjorth ⓘ https://orcid.org/0000-0002-4571-2306
T.-W. Chen ⓘ https://orcid.org/0000-0002-1066-6098
M. Nicholl ⓘ https://orcid.org/0000-0002-2555-3192
R. J. Foley ⓘ https://orcid.org/0000-0002-2445-5275
A. Rest ⓘ https://orcid.org/0000-0002-4410-5387
K. W. Smith ⓘ https://orcid.org/0000-0001-9535-3199
D. R. Young ⓘ https://orcid.org/0000-0002-1229-2499
S. A. Sim ⓘ https://orcid.org/0000-0002-9774-1192
Y. Zenati ⓘ https://orcid.org/0000-0002-0632-8897
H. Gao ⓘ https://orcid.org/0000-0003-1015-5367
C.-C. Lin ⓘ https://orcid.org/0000-0002-7272-5129
T. Lowe ⓘ https://orcid.org/0000-0002-9438-3617
E. A. Magnier ⓘ https://orcid.org/0000-0002-7965-2815
I. A. Smith ⓘ https://orcid.org/0000-0001-8605-5608
R. Wainscoat ⓘ https://orcid.org/0000-0002-1341-0952
D. A. Coulter ⓘ https://orcid.org/0000-0003-4263-2228
D. O. Jones ⓘ https://orcid.org/0000-0002-6230-0151
C. D. Kilpatrick ⓘ https://orcid.org/0000-0002-5740-7747
P. McGill ⓘ https://orcid.org/0000-0002-1052-6749
E. Ramirez-Ruiz ⓘ https://orcid.org/0000-0003-2558-3102
K.-S. Lee ⓘ https://orcid.org/0000-0003-3004-9596
G. Narayan ⓘ https://orcid.org/0000-0001-6022-0484
V. Ramakrishnan ⓘ https://orcid.org/0000-0002-9176-7252
R. Ridden-Harper ⓘ https://orcid.org/0000-0003-1724-2885
Q. Wang ⓘ https://orcid.org/0000-0001-5233-6989
A. K. H. Kong ⓘ https://orcid.org/0000-0002-5105-344X
C.-C. Ngeow ⓘ https://orcid.org/0000-0001-8771-7554
Y.-C. Pan ⓘ https://orcid.org/0000-0001-8415-6720
S. Yang ⓘ https://orcid.org/0000-0002-2898-6532
K. W. Davis ⓘ https://orcid.org/0000-0002-5680-4660
A. L. Piro ⓘ https://orcid.org/0000-0001-6806-0673
C. Rojas-Bravo ⓘ https://orcid.org/0000-0002-7559-315X
J. Sommer ⓘ https://orcid.org/0000-0002-1154-8317
S. K. Yadavalli ⓘ https://orcid.org/0000-0002-0840-6940

References

Arnett, W. D. 1982, ApJ, 253, 785
Ashall, C., Mazzali, P. A., Pian, E., et al. 2019, MNRAS, 487, 5824
Astropy Collaboration, Price-Whelan, A. M., Lim, P. L., et al. 2022, ApJ, 935, 167

Astropy Collaboration, Price-Whelan, A. M., Sipőcz, B. M., et al. 2018, AJ, 156, 123
Astropy Collaboration, Robitaille, T. P., Tollerud, E. J., et al. 2013, A&A, 558, A33
Baktash, A., Horns, D., & Meyer, M. 2022, arXiv:2210.07172
Bazin, G., Palanque-Delabrouille, N., Rich, J., et al. 2009, A&A, 499, 653
Bissaldi, E., Omodei, N., Kerr, M. & Fermi-LAT Team 2022, GCN, 32637, 1
Bradley, L., Sipőcz, B., Robitaille, T., et al. 2022, astropy/photutils: v1.5.0, Zenodo, doi:10.5281/zenodo.6825092
Bright, J., Rhodes, L., Fender, R., et al. 2022, GCN, 32653, 1
Campana, S., Lazzati, D., Perna, R., Grazia Bernardini, M., & Nava, L. 2021, A&A, 649, A135
Cano, Z., Wang, S.-Q., Dai, Z.-G., & Wu, X.-F. 2017a, AdAst, 2017, 8929054
Cano, Z., Izzo, L., de Ugarte Postigo, A., et al. 2017b, A&A, 605, A107
Carenza, P., & Marsh, M. C. D. 2022, arXiv:2211.02010
Castro-Tirado, A. J., Sanchez-Ramirez, R., Hu, Y. D., et al. 2022, GCN, 32686, 1
Chambers, K. C., Magnier, E. A., Metcalfe, N., et al. 2016, arXiv:1612.05560
Chandra, P., & Frail, D. A. 2012, ApJ, 746, 156
Chen, T. W., Malesani, D. B., Yang, S., et al. 2022, GCN, 32667, 1
Chugai, N. N. 2000, AstL, 26, 797
Coulter, D. A., Jones, D. O., McGill, P., et al. 2022, YSE-PZ: An Open-source Target and Observation Management System, v0.3.0, Zenodo, doi:10.5281/zenodo.7278430
de Ugarte Postigo, A., Izzo, L., Pugliese, G., et al. 2022, GCN, 32648, 1
Della Valle, M., Chincarini, G., Panagia, N., et al. 2006, Natur, 444, 1050
Dichiara, S., Gropp, J., Kennea, J., et al. 2022, GCN, 32632, 1
Dolphin, A. 2016, DOLPHOT: Stellar photometry, Astrophysics Source Code Library, ascl:1608.013
Dzhappuev, D. D., Afashokov, Y. Z., Dzaparova, I. M., et al. 2022, ATel, 15669, 1
Evans, P. A., Beardmore, A. P., Page, K. L., et al. 2007, A&A, 469, 379
Evans, P. A., Beardmore, A. P., Page, K. L., et al. 2009, MNRAS, 397, 1177
Evans, P. A., Willingale, R., Osborne, J. P., et al. 2010, A&A, 519, A102
Fitzpatrick, E. L. 1999, PASP, 111, 63
Flewelling, H. A., Magnier, E. A., Chambers, K. C., et al. 2020, ApJS, 251, 7
Fukugita, M., Ichikawa, T., Gunn, J. E., et al. 1996, AJ, 111, 1748
Fynbo, J. P. U., Watson, D., Thöne, C. C., et al. 2006, Natur, 444, 1047
Galama, T. J., Vreeswijk, P. M., van Paradijs, J., et al. 1998, Natur, 395, 670
Granot, J., & Sari, R. 2002, ApJ, 568, 820
Guillochon, J., Nicholl, M., Villar, V. A., et al. 2018, ApJS, 236, 6

Hjorth, J., & Bloom, J. S. 2012, in Gamma-ray Bursts, ed. C. Kouveliotou, R. A. M. J. Wijers, & Stan Woosley (Cambridge: Cambridge Univ. Press), 169
Hjorth, J., Sollerman, J., Møller, P., et al. 2003, Natur, 423, 847
Huang, Y., Hu, S., Chen, S., et al. 2022, GCN, 32677, 1
Huber, M., Schultz, A., Chambers, K. C., et al. 2022, GCN, 32758, 1
Iwamoto, K., Mazzali, P. A., Nomoto, K., et al. 1998, Natur, 395, 672
Izzo, L., de Ugarte Postigo, A., Maeda, K., et al. 2019, Natur, 565, 324
Izzo, L., Saccardi, A., Fynbo, J. P. U., et al. 2022, GCN, 32765, 1
Jones, D. O., Foley, R. J., Narayan, G., et al. 2021, ApJ, 908, 143
Kann, D. A., Agayeva, S., Aivazyan, V., et al. 2023, ApJL, submitted
Kennea, J. A., Williams, M., & & Swift Team 2022, GCN, 32635, 1
Laskar, T., Alexander, K. D., Margutti, R., et al. 2023, ApJL, in press
Leśniewska, A., Michałowski, M. J., Kamphuis, P., et al. 2022, ApJS, 259, 67
Levan, A., Barclay, T., Bhirombhakdi, K., et al. 2022, GCN, 32921, 1
Levan, A. J., Lamb, G. P., Schneider, B., et al. 2023, ApJL, submitted
Magnier, E. A., Chambers, K. C., Flewelling, H. A., et al. 2020a, ApJS, 251, 3
Magnier, E. A., Schlafly, E. F., Finkbeiner, D. P., et al. 2020b, ApJS, 251, 6
Mazzali, P. A., Deng, J., Tominaga, N., et al. 2003, ApJL, 599, L95
McBrien, O. R., Smartt, S. J., Huber, M. E., et al. 2021, MNRAS, 500, 4213
Melandri, A., Izzo, L., Pian, E., et al. 2022, A&A, 659, A39
Miknaitis, G., Pignata, G., Rest, A., et al. 2007, ApJ, 666, 674
NASA/IPAC Extragalactic Database (NED) 2019, NED Extinction Calculator, IPAC, doi:10.26132/NED5
Patat, F., Cappellaro, E., Danziger, J., et al. 2001, ApJ, 555, 900
Perley, D. 2022, GCN, 32638, 1
Postigo, A. D. U., Izzo, L., Thoene, C. C., et al. 2022, TNSCR, 2022-3047, 1
Rastinejad, J. C., Gompertz, B. P., Levan, A. J., et al. 2022, Natur, 612, 223
Rest, A., Scolnic, D., Foley, R. J., et al. 2014, ApJ, 795, 44
Rest, A., Stubbs, C., Becker, A. C., et al. 2005, ApJ, 634, 1103
Rhodes, L., van der Horst, A. J., Fender, R., et al. 2022, MNRAS, 513, 1895
Sari, R., Piran, T., & Narayan, R. 1998, ApJL, 497, L17
Schlafly, E. F., & Finkbeiner, D. P. 2011, ApJ, 737, 103
Shrestha, M., Sand, D. J., Alexander, K. D., et al. 2023, arXiv:2302.03829
Smith, K. W., Smartt, S. J., Young, D. R., et al. 2020, PASP, 132, 085002
Speagle, J. S. 2020, MNRAS, 493, 3132
Tonry, J. L., Stubbs, C. W., Lykke, K. R., et al. 2012, ApJ, 750, 99
Veres, P., Burns, E., Bissaldi, E., et al. 2022, GCN, 32636, 1
Villar, V. A., Berger, E., Metzger, B. D., & Guillochon, J. 2017, ApJ, 849, 70
Virtanen, P., Gommers, R., Oliphant, T. E., et al. 2020, NatMe, 17, 261
Waters, C. Z., Magnier, E. A., Price, P. A., et al. 2020, ApJS, 251, 4
Wheeler, J. C., Johnson, V., & Clocchiatti, A. 2015, MNRAS, 450, 1295